Molecular Neurobiology (2019) 56:321–334
https://doi.org/10.1007/s12035-018-1078-9

# Impaired Bioenergetics in Mutant Mitochondrial DNA Determines Cell Fate During Seizure-Like Activity

Stjepana Kovac[1,2] · Elisavet Preza[3] · Henry Houlden[3] · Matthew C. Walker[1] · Andrey Y. Abramov[3]

Received: 18 February 2018 / Accepted: 10 April 2018 / Published online: 27 April 2018


## Abstract

Mutations in genes affecting mitochondrial proteins are increasingly recognised in patients with epilepsy, but the factors determining cell fate during seizure activity in these mutations remain unknown. Fluorescent dye imaging techniques were applied to fibroblast cell lines from patients suffering from common mitochondrial mutations and to age-matched controls. Using live cell imaging techniques in fibroblasts, we show that fibroblasts with mutations in the mitochondrial genome had reduced mitochondrial membrane potential and NADH pools and higher redox indices, indicative of respiratory chain dysfunction. Increasing concentrations of ferutinin, a $Ca^{2+}$ ionophore, led to oscillatory $Ca^{2+}$ signals in fibroblasts resembling dynamic $Ca^{2+}$ changes that occur during seizure-like activity. Co-monitoring of mitochondrial membrane potential ($\Delta\Psi_m$) changes induced by ferutinin showed accelerated membrane depolarisation and cell collapse in fibroblasts with mutations in the mitochondrial genome when compared to controls. $Ca^{2+}$ flash photolysis using caged $Ca^{2+}$ confirmed impaired $Ca^{2+}$ handling in fibroblasts with mitochondrial mutations. Findings indicate that intracellular $Ca^{2+}$ levels cannot be compensated during periods of hyperexcitability, leading to $Ca^{2+}$ overload and subsequent cell death in mitochondrial diseases.

**Keywords** Epilepsy · Fibroblasts · Mitochondrial mutation · $Ca^{2+}$ · PTP opening

## Introduction

Mutations in genes affecting mitochondrial proteins are increasingly recognised as a cause of human disease as genetic tools become more widely available in clinical practice [1]. Although there is strong associational data between gene mutations and specific phenotypes, the functional consequences of these mutations remain less clear.

Mutations are not distributed evenly across the mitochondrial genome, but several hotspots exist. Such hotspots are seen in mitochondrial DNA coding for transfer RNA (tRNA) [2]. The m.3243A>G MT-TL1 gene mutation and the 8344A>G MT-TK gene mutation both affect tRNA and are frequently encountered in human disease. M.3243A>G MT-TL1 gene mutations present mitochondrial encephalopathy with lactic acidosis and stroke-like episodes (MELAS). This particular mutation accounts for 80% of cases with MELAS [3]. Similarly, the 8344A>G MT-TK gene mutation is another hotspot and accounts for 80% of cases presenting with myoclonic epilepsy with ragged red fibres (MERRF) [4].

A common feature in mitochondrial disease, and also in the two above-described syndromes, is network hyperexcitability, leading to seizures. Indeed, epilepsy is an important aspect of mitochondrial disease and contributes significantly to morbidity [5, 6].

We have previously shown that hyperexcitability in cellular epilepsy models affects $Ca^{2+}$ handling in mitochondria and ROS homeostasis, ultimately altering energy homeostasis in neurons [7–9]. It is possible that similar mechanisms apply to hyperexcitability and seizures seen in patient suffering from mitochondrial mutations, but such evidence is lacking.

**Electronic supplementary material** The online version of this article (https://doi.org/10.1007/s12035-018-1078-9) contains supplementary material, which is available to authorized users.

✉ Stjepana Kovac
stjepana.kovac@ukmuenster.de

✉ Andrey Y. Abramov
a.abramov@ucl.ac.uk

[1] Department of Clinical and Experimental Epilepsy, UCL Institute of Neurology, University College London, London, UK

[2] Department of Neurology, University of Muenster, Muenster, Germany

[3] Department of Molecular Neuroscience, UCL, London, UK

One approach to address these questions would be to create networks of neurons from reprogrammed cell lines. However, there are problems inherent to cell reprogramming including determining cell identity and generating networks that can maintain seizure-like activity.

Several lines of evidence suggest that calcium ($Ca^{2+}$) handling is impaired in different types of cells with mitochondrial mutations and not only in neurons [10, 11]. This is not surprising and is likely due to the fact that mitochondrial $Ca^{2+}$ handling is a process which is conserved among vertebral species and, more importantly, between different tissues [12]. It implies that mitochondrial pathologies and functions can be studied in different tissues. This is supported by a study investigating neurons derived from various *cybrid* embryonic stem cell lines harbouring mutations in complexes I and IV [11]. Interestingly, this study found similar $Ca^{2+}$-handling deficits in neurons and fibroblasts of patients with MELAS syndrome, suggesting that the cellular pathology in mitochondrial disease might be reflected in many different cell types but also in fibroblasts and, thus, fibroblasts seem to faithfully reproduce the disease phenotype.

We have thus taken an alternative approach that is robust and easy to implement and so lends itself to large-scale drug screening. In this study, we determined the mechanisms underlying impaired $Ca^{2+}$ handling in mitochondrial disease using human fibroblasts as a disease model. Human fibroblasts have a different system of ion channels participating in signal transmission. To address this, we induced large intracellular $Ca^{2+}$ transients (such as those occurring during seizure activity) in these cells using $Ca^{2+}$ ionophores and caged $Ca^{2+}$.

## Results

### Identification of Mitochondrial Pathology in Patients' Fibroblasts

The mitochondrial membrane potential ($\Delta\Psi_m$) is a universal indicator of mitochondrial integrity and function. Alterations of $\Delta\Psi_m$ are a marker of mitochondrial disease pathology. We therefore compared basal $\Delta\Psi_m$ in fibroblasts with mitochondrial mutations to those of age-matched controls. There was a

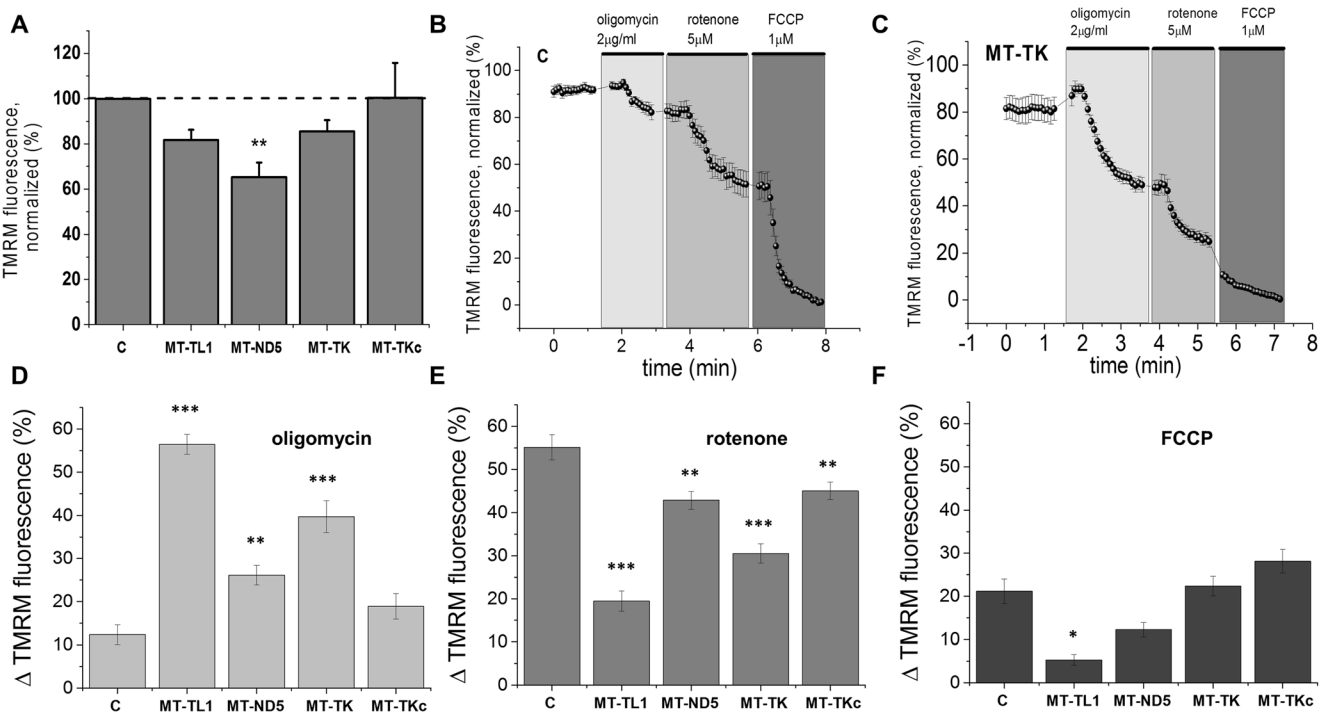


**Fig. 1** Mitochondrial membrane potential in fibroblasts with mitochondrial mutations. Mitochondrial membrane potential ($\Delta\Psi_m$) is depolarised in fibroblast cell lines harbouring mitochondrial mutations when compared to control cell lines (**a**), and $\Delta\Psi_m$ is maintained at the expense of respiration in some mitochondrial mutations (**b**–**f**). Representative experiments from control (**b**) fibroblasts and fibroblasts harbouring mitochondrial mutations (**c**; MT-TK mutation). Data indicate mean and SEM of TMRM fluorescence in fibroblasts in a representative experiment. Traces are normalised with 100% set as baseline TMRM fluorescence and 0% set as fluorescence after complete depolarisation of $\Delta\Psi_m$ with FCCP. Note that oligomycin profoundly decreases TMRM fluorescence in mitochondrial mutations (**c**) whereas this effect is not visible in control fibroblasts (**b**, **d**). $\Delta\Psi$m is expressed as TMRM fluorescence. High TMRM fluorescence intensities indicate relative hyperpolarisation whereas low fluorescence indicates depolarisation. Bar charts summarising mean (±SEM) changes in fluorescence in percentages after treatment with oligomycin (**d**), rotenone (**e**) and FCCP (**f**) in different cell lines. Data in **a** is normalised to the control (**c**) cell line. Note that $\Delta\Psi_m$ is reduced in fibroblasts with mitochondrial mutations (MT-TL1; MT-ND5 and MT-TK) when compared to control (C), but not in fibroblasts from the unaffected mother (MT-TKc). Error bars indicate SEM. $^{**}p < 0.01$;$^{**}$ $p < 0.001$

statistically significant difference in the ΔΨm between the groups as measured with tetramethylrhodamine methyl ester (TMRM) ($F(4, 23) = 6.380$; $p < 0.01$; one-way ANOVA; Fig. 1a). ΔΨm was ~15–20% lower in tRNA mutations (MT-TL1 and MT-TK) and ~40% lower in complex I mutation (MT-ND5) when compared to that in control (C).

Next, we investigated how robust ΔΨm is in fibroblasts when challenged with oligomycin and rotenone, potent inhibitors of mitochondrial complexes V and I. This was done by assessing the drop in TMRM fluorescence and, thus, the degree of depolarisation of the mitochondrial membrane potential after application of oligomycin and rotenone. To assess the functional reserve of the ΔΨm, the mitochondrial uncoupler carbonyl cyanide-*p*-trifluoromethoxyphenylhydrazone (FCCP; 1 μM) was added after application of those inhibitors, which, in all experiments, led to complete depolarisation of ΔΨm, i.e. loss of TMRM fluorescence (Fig. 1b, c). There was a statistically significant difference in the magnitude of $\Delta\Psi_m$ drop (ΔTMRM) between the different cell lines after the addition of oligomycin (Fig. 1d, $F(4, 166) = 30.95$; $p < 0.001$; one-way ANOVA), rotenone (Fig. 1e, $F(4, 166) = 26.24$; $p < 0.001$; one-way ANOVA) and FCCP (Fig. 1f, $F(4, 166) = 9.30$; $p < 0.001$; one-way ANOVA). Control cells showed only a mild drop in $\Delta\Psi_m$ of around 10% of the total mitochondrial membrane potential in response to the $F_1F_0$-ATP synthase inhibitor oligomycin (0.2 μg/ml; Fig. 1b, d), while mitochondria in mutated cells showed the marked depolarisation of $\Delta\Psi_m$ in response to oligomycin, ranging from 25 to 70% (post hoc Dunnett's test; Fig. 1d). Subsequent inhibition of complex I by rotenone (5 μM) caused a rapid loss of potential which also differed in its magnitude between the cell lines (post hoc Dunnett's test; Fig. 1b, c, f). Control cells showed the most marked depolarisation after rotenone application reaching ~55% of $\Delta\Psi_m$, whereas in cells with mitochondrial mutations, depolarisation with rotenone was less pronounced ranging from ~20 to 45% (Fig. 1f). This is likely due to the fact that in those cells, inhibition of complex V with oligomycin already yielded a marked depolarisation. Finally, the depolarization of $\Delta\Psi_m$ after complex I and complex V inhibition, as assessed with FCCP, showed also marked differences between the groups (post hoc Dunnett's test; Fig. 1b, c, f). These findings imply that the ΔΨm in fibroblasts with the mitochondrial mutations is maintained by complex V working in reverse mode and, thus, at the expense of respiration and oxidative phosphorylation.

## Basal NADH Levels and Redox Index in Fibroblasts with Mitochondrial Mutations

NADH is a complex I substrate. The redox index of NADH expresses the ratio of maximally oxidised and maximally reduced NADH states within the mitochondria. Maximal oxidation is stimulated by treatment with mitochondrial uncoupler FCCP. Maximal reduction is established by inhibiting respiration with NaCN (for examples, see Fig. 2a, c). The redox state, therefore, is a measure of the activity of the mitochondrial electron transport chain.

We found that there was a statistically significant difference in the NADH levels between the different groups ($F(4, 15) = 14.69$; $p < 0.001$; one-way ANOVA; Fig. 2b). The reduction in NADH levels varied between ~20% in fibroblasts with MT-ND5 mutations ($p = 0.027$; post hoc Dunnett's test) and ~30% in fibroblasts with MT-TL1 mutation ($p = 0.003$; post hoc Dunnett's test) and was most prominent in fibroblasts with MT-TK mutations showing a reduction of ~60% ($p < 0.001$; post hoc Dunnett's test; Fig. 2b) compared to control. There was no difference between the control and the fibroblasts from the unaffected mother ($MT\text{-}TK_c$). The reduction in mitochondrial NADH pool may be explained by higher consumption of NADH via complex I or by a slower rate of production of this molecule in the tricarboxylic acid (TCA) cycle. Thus, we next established the redox indices. In a one-way ANOVA, we found a significant difference in the redox index between the groups ($F(4, 18) = 3.60$; $p < 0.05$). The redox index was increased when compared to control. This increase varied from ~15 to 30%. Post hoc analysis revealed that this reached statistical significance for fibroblasts harbouring the MT-TK mutation ($p = 0.007$; post hoc Dunnett's test; Fig. 2d). An increased redox index indicates lower activity of the complex I activity in fibroblasts with mitochondrial mutation confirming their impaired respiration. Lower NADH pools in cells harbouring mitochondrial mutations when compared to control cells and decreased activity of complex I-related respiration as expressed by the redox index suggest partial inhibition of NADH production in TCA cycle.

## Mitochondrial Mass

Mitochondrial dysfunction and energy deprivation in some cells can be compensated by increased mitochondrial biogenesis. However, there was no statistically significant difference in the mitochondrial mass that varied between 9 and 14 vol% of the cell between fibroblasts with different mitochondrial mutations and controls ($F(4, 17) = 14.73$; $p = 0.194$; one-way ANOVA; Suppl. Fig. 1).

## Dynamic $Ca^{2+}$ Handling in Cells with Mitochondrial Mutations

Network hyperexcitability in mitochondrial disease can result in seizures and epilepsy. Such hyperexcitability is critically dependent on $Ca^{2+}$ homeostasis within the cell with the mitochondria playing a major role in $Ca^{2+}$ homeostasis [7, 13]. Unsurprisingly, the mutations investigated here presented with seizures as a prominent phenotype (see Suppl. Table 1). We therefore investigated whether dynamic $Ca^{2+}$ handling, which is required in situations with large intracellular $Ca^{2+}$

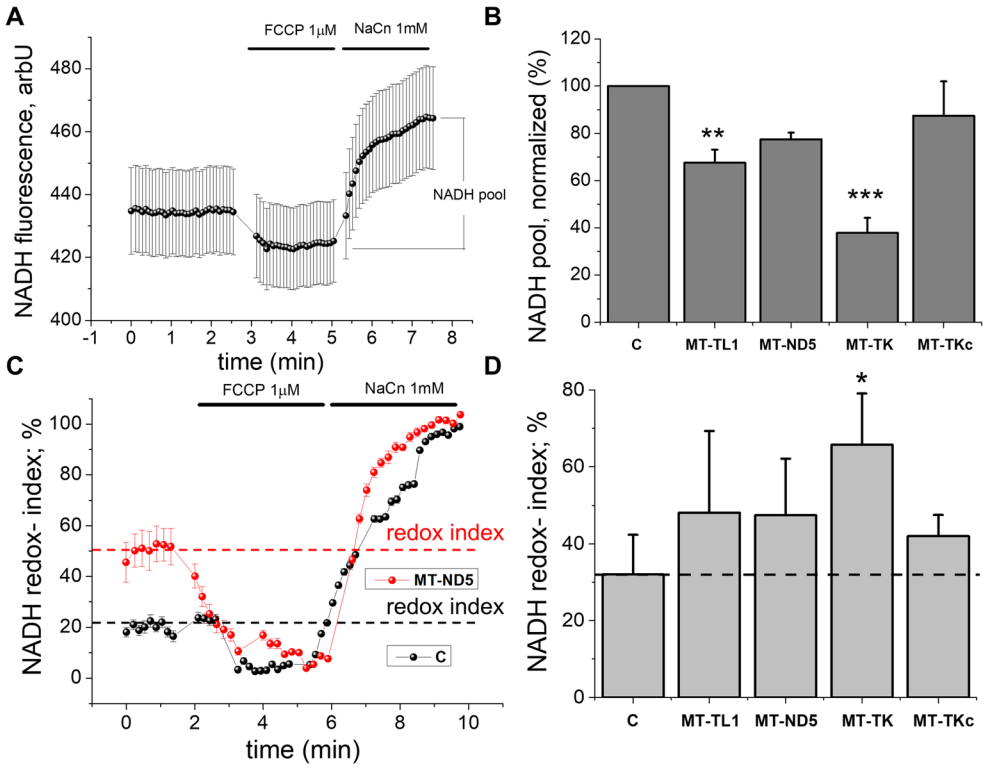


**Fig. 2** NADH pools are low, and NADH redox indices are decreased in fibroblasts with mitochondrial mutations, suggesting inhibition of respiration. NADH autofluorescence was measured after supramaximal stimulation of respiration with FCCP (1μM) and inhibition of respiration with NaCN (1 mM; **a**, **c**). NADH pools were determined as the magnitude of fluorescence change between supramaximal stimulation and inhibition of respiration (**a**). Bar charts showing mean (±SEM) NADH pools of the fibroblast cell lines (**b**). Data normalised to control (set as 100%). Redox indices were determined as the ratio of maximally oxidised and maximally reduced NADH states and can be determined after supramaximal stimulation of respiration with FCCP and inhibition of respiration with NaCN. Redox indices are given in percentages. Bar chart comparing mean (±SD) redox indices (**d**). **a**, **c** Representative experiments. Traces in **a**, **c** represent the mean and SEM of fibroblasts within one experiment. Note that NADH pools are reduced in fibroblast cell lines with mitochondrial mutations and that redox indices are high, indicating deficient respiration; $*p < 0.05$; $**p < 0.01$; $***p < 0.001$.

rises as seen in seizures [7], is impaired in fibroblasts with mitochondrial mutations.

In addition, mitochondrial dehydrogenases (including NADH dehydrogenase) are $Ca^{2+}$-dependent enzymes [14]. Mitochondrial $Ca^{2+}$ uptake regulates respiration, and as result, increases in mitochondrial $Ca^{2+}$ uptake lead to increased ATP production [15]. Mitochondrial $Ca^{2+}$ capacity is a key element in the regulation of the mitochondrial permeability transition pore (MPTP). We thus quantified mitochondrial $Ca^{2+}$ pools. We also quantified endoplasmic reticulum (ER) $Ca^{2+}$ pools since these are closely linked to mitochondrial $Ca^{2+}$ signalling [16]. We estimated these by stimulating $Ca^{2+}$ release from the ER with 1 μM thapsigargin and, subsequently, by depleting mitochondrial $Ca^{2+}$ with 1 μM ionomycin (Fig. 3a) in nominally $Ca^{2+}$-free external medium. We found a significant difference in ER $Ca^{2+}$ pools as estimated by fura-2 ratios between the fibroblast cell lines ($F(4, 475) = 19.14$; $p < 0.001$; one-way ANOVA). Similarly, mitochondrial $Ca^{2+}$ pools varied significantly between the fibroblast cell lines ($F(4, 476) = 33.07$; $p < 0.001$; one-way ANOVA). In fibroblasts with complex I mutation (MT-ND5), mitochondrial $Ca^{2+}$ pools were smaller whereas ER $Ca^{2+}$ pools were larger when compared to control (Fig. 3b, c). Interestingly, the reverse was observed with MT-TK mutations. MT-TL1 mutations did not show any differences in either ER or mitochondrial $Ca^{2+}$ pools when compared to control.

We next explored different models to assess $Ca^{2+}$ handling in fibroblasts with mitochondrial mutations. Unlike excitatory cells such as neurons, fibroblasts are cells specialised to synthesise extracellular matrix and, as such, lack the receptor composition found on neurons. We and others have highlighted a critical role of NMDA receptor-mediated $Ca^{2+}$ toxicity during seizure activity [7, 17].

We therefore sought to model repetitive $Ca^{2+}$ changes using pharmacological tools. Ferutinin, a naturally occurring terpenoid, has $Ca^{2+}$ ionophoretic properties by increasing cation permeability of cells and mitochondria in a dose-dependent manner [18, 19]. Ferutinin therefore contributes to MPTP opening via $Ca^{2+}$ overload [20]. We have previously found that MPTP opening contributes to neuronal cell death in hyperexcitability [7]. We found that increasing concentrations of ferutinin lead to oscillatory $Ca^{2+}$ signals in the cytosol

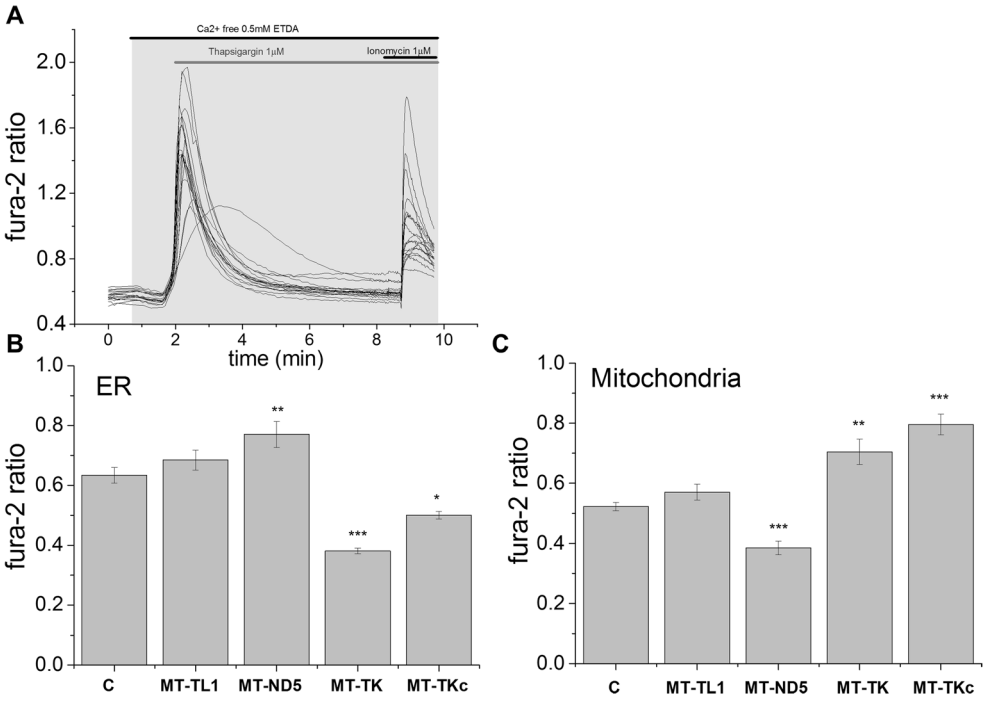


**Fig. 3** Mitochondrial $Ca^{2+}$ stores and $Ca^{2+}$ stores in the endoplasmatic reticulum in different fibroblasts cell lines. Method used to estimate cellular $Ca^{2+}$ stores (**a**). Each trace represents cytoplasmic $Ca^{2+}$ measurements in a single fibroblast. $Ca^{2+}$ stores were estimated in $Ca^{2+}$-free media by adding thapsigargin (1 μM) to estimate $Ca^{2+}$ stores in the endoplasmatic reticulum and by adding ionomycin (1 μM) to measure mitochondrial $Ca^{2+}$ stores. Bar charts summarising endoplasmatic reticulum (**b**) and mitochondrial (**c**) $Ca^{2+}$ stores as measured with fura-2. $*p < 0.05$; $**p < 0.01$; $***p < 0.001$

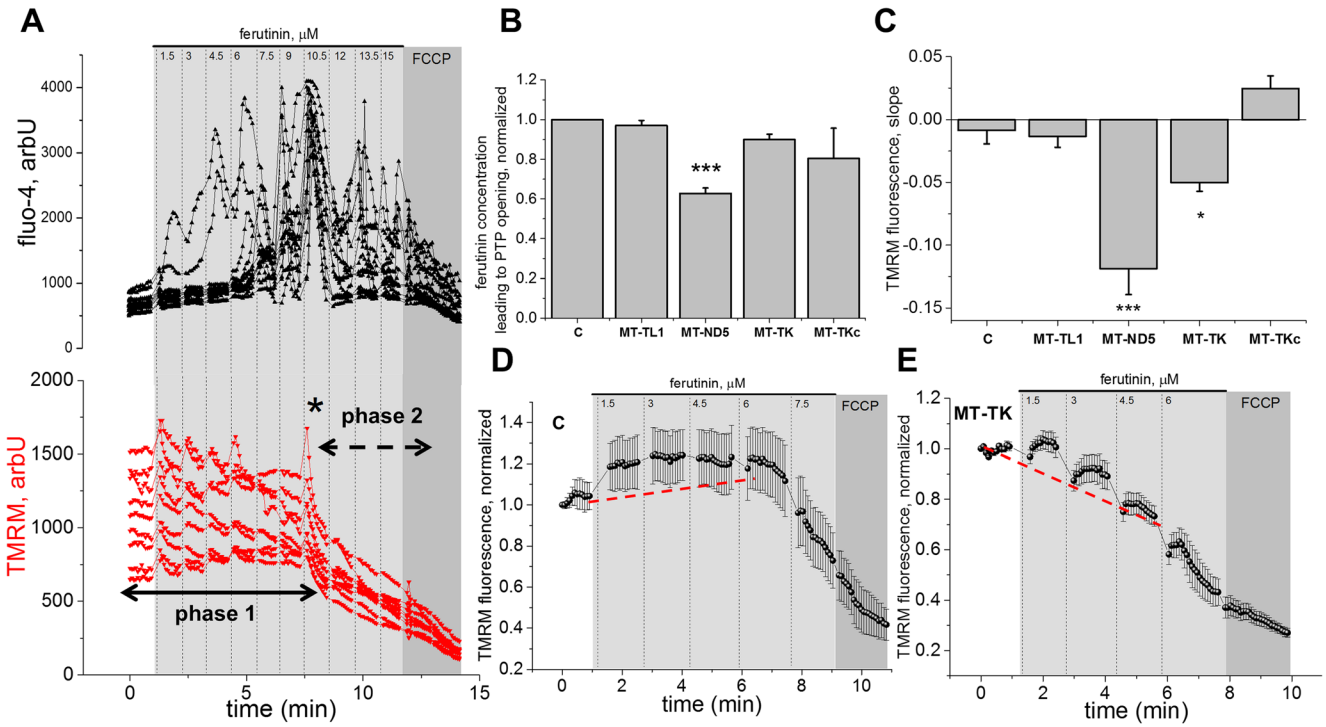


**Fig. 4** Dynamic $Ca^{2+}$ handling in fibroblasts with mitochondrial mutations. $Ca^{2+}$ signal as measured with fluo-4 (**a**; upper panel) and corresponding $\Delta\Psi_m$ changes as measured with TMRM in fibroblasts (**a**; lower panel) after treatment with ferutinin in increasing concentrations. Each trace shown in **a** represents fluo-4 (upper panel) or TMRM (lower panel) signal measured in one fibroblast. Note that two distinct phases of TMRM signal can be distinguished based on the shape of the signal. Phase 1 is characterised by a mild decrease in TMRM fluorescence. In phase 2, which coincides with an increase in intracellular $Ca^{2+}$, a rapid decrease in TMRM fluorescence is observed, suggesting mitochondrial permeability transition pore (MPTP) opening. The ferutinin concentration used to initiate MPTP opening was considered the threshold concentration (single asterisk indicates this concentration). Bar chart summarising mean (±SEM) threshold concentrations, leading to MPTP opening in different fibroblast cell lines (data normalised to control; **b**). Bar chart summarising mean (±SEM) slopes of TMRM fluorescence change in fibroblast cell lines (**c**). Representative traces of mean TMRM fluorescence during ferutinin application in control fibroblasts (**d**) and fibroblasts with mitochondrial mutation (MT-TK; **e**). $***p < 0.001$

(Fig. 4a, upper panel). These signals were accompanied by changes in the ΔΨm (Fig. 4a, lower panel). Qualitative analysis of the ΔΨm changes induced by increasing concentrations of ferutinin identified two distinct phases: (1) a phase which was characterised by a relatively stable $\Delta\Psi_m$ or only minor $\Delta\Psi_m$ changes and (2) a time point with accelerated $\Delta\Psi_m$ changes (see Fig. 4a). This acceleration coincided with a steep increase in the $Ca^{2+}$ signal (see fluo-4 trace) and could be visualised as either decreased TMRM fluorescence as measured over the mitochondria or increased TMRM fluorescence over the nuclei. The nuclei exhibit a transient increase of TMRM fluorescence once the dye is redistributed (Suppl. Fig. 2). We interpreted this steep decline in $\Delta\Psi_m$ as MPTP opening. Comparison of different fibroblast cell lines showed that MPTP opening (phase 2), measured as peak fluorescence over cell nuclei, differed ($F(4, 82) = 23.23$; $p < 0.001$; one-way ANOVA). Post hoc analysis showed that this difference was sustained by a significantly accelerated MPTP opening in fibroblasts with complex I mutations (MT-ND5; $p < 0.001$; post hoc Dunnett's test; Fig. 4b). There was a trend toward earlier MPTP opening in the MT-TK cell line when compared to control ($p = 0.054$; post hoc Dunnett's test). We next analysed the slope of TMRM fluorescence change measured over the mitochondria representing the initial phase (phase 1) defined by a slow decline in $\Delta\Psi_m$. We found a significant difference between the cell lines ($F(4, 102) = 13.64$; $p < 0.001$; one-way ANOVA; Fig. 4c). Post hoc analysis showed that there was a steep phase 1 decline in $\Delta\Psi_m$ of fibroblasts with complex I mutations (MT-ND5; $p < 0.001$; post hoc Dunnett's test) and also a significant decline in ΔΨm in fibroblasts with MT-TK tRNA mutations ($p = 0.036$; post hoc Dunnett's test) when compared to control (Fig. 4c–e). Altogether, there was a clear dose-dependent effect of ferutinin on $\Delta\Psi_m$ with increasing concentrations within the experiment, leading both to MPTP opening and affecting the slope (and thus, $\Delta\Psi_m$) of the signal (see Fig. 4a). The final concentration needed to induce MPTP opening varied slightly between experimental days, and thus, the data was normalised to the value obtained with the control fibroblast cell line obtained on one experimental day (Fig. 4b).

To model repetitive $Ca^{2+}$ oscillations in fibroblast—as those seen in neurons during seizure-like activity (Fig. 5a, b)—we loaded cells with the photolabile $Ca^{2+}$ chelator *o*-nitrophenyl ethylene glycol tetraacetic acid (NP-EGTA; caged $Ca^{2+}$). Upon UV exposure, $Ca^{2+}$ is released into the cell. We then studied the effect of $Ca^{2+}$ challenge imposed by this technique on one mutation with a very profound effect (MT-ND5) and one with no effect (MT-TL1) on $Ca^{2+}$ handling as assessed in the experiments with the $Ca^{2+}$ ionophore ferutinin. We found that repetitive UV-induced $Ca^{2+}$ release in cells leads to a depolarisation of the ΔΨm in fibroblasts (Fig. 5e). This depolarisation was not observed in adjacent cells not exposed to UV light (Fig. 5d). We applied this method to control fibroblasts and fibroblasts with MT-TL1 and MT-ND5 mutations. We found a steady decrease in the ΔΨm indicated by a TMRM fluorescence decrease during $Ca^{2+}$ flash photolysis (Fig. 6a) in cells harbouring mitochondrial mutations. This correlated to an increase in TMRM fluorescence over the nucleus. TMRM signals in nuclei were quantified, given the difficulties measuring fluorescence over a single mitochondrion due to movement. There was a statistically significant difference in mitochondrial membrane potential depolarisation after repetitive $Ca^{2+}$ challenge between control fibroblasts ($n = 9$ cells) and fibroblasts harbouring the MT-TL1 mutation ($n = 7$; $p < 0.001$; *t*-test) or fibroblasts harbouring the MT-ND5 mutation ($n = 7$; $p < 0.001$; *t*-test; Fig. 6b–e).

## ATP Depletion in Fibroblasts with Mitochondrial Mutations

Mitochondrial $Ca^{2+}$ uptake is electrogenic and thus leads to a depolarisation of the mitochondrial membrane potential. The mitochondrial membrane potential is the driving force of ATP production and is dependent on a hyperpolarised mitochondrial membrane potential. Taken together, this suggests that mitochondrial $Ca^{2+}$ uptake is an energy-depleting process.

We have previously demonstrated that $Ca^{2+}$ oscillations induced by low $Mg^{2+}$ seizure-like activity led to energy deprivation and cell death [7]. To investigate whether metabolic changes observed in fibroblasts with mitochondrial mutations are linked to ATP depletion, we investigated ATP levels measured with Mag-fura after challenging fibroblasts with ferutinin in a glucose-deprived environment. Fibroblasts are glycolytic cells while neurons are not. Thus, we made use of glucose deprivation of the external medium to eliminate glycolysis as a source of ATP production, to be able to focus on mitochondrial ATP production. Mag-fura allows real-time imaging of changes in ATP as intracellular magnesium concentrations are closely linked to ATP levels—free $[Mg^{2+}]_c$ increases during ATP depletion through hydrolysis of $Mg^{2+}$ ATP [21]. We first determined threshold concentrations of ferutinin which would lead to ATP depletion in fibroblasts. Stepwise increases in ferutinin concentration showed that 40–50 μM was the concentration required to induce rapid ATP changes in fibroblasts in a glucose-deprived environment (Fig. 7a, b). We then measured the delay in ATP depletion after application of 40 μM ferutinin in the different fibroblast cell lines. In a one-way ANOVA, we found a significant difference in the delay to ATP depletion ($F(4, 211) = 23.8$; $p < 0.001$). Post hoc analysis revealed that fibroblasts harbouring the MT-TK mutation had faster ATP depletion compared to the other cell lines ($p < 0.001$; post hoc Dunnett's test; Fig. 7c–e).

## Discussion

Studying mitochondrial function and the impact of disease pathophysiology on mitochondrial function is a challenge.

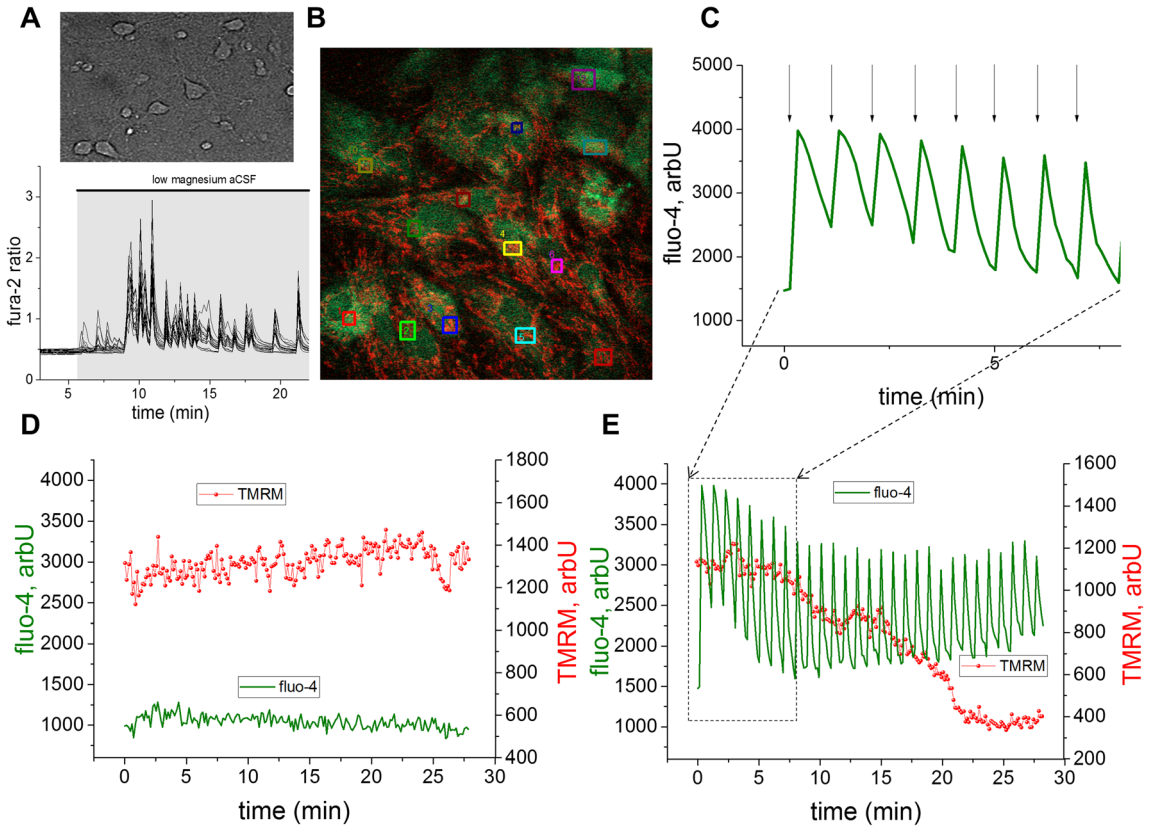


**Fig. 5** Modelling hyperexcitability induced dynamic $Ca^{2+}$ changes in fibroblasts with caged $Ca^{2+}$. Phase-contrast image of neurons in cultures (**a**; upper panel) and repetitive $Ca^{2+}$ oscillations measured in neurons during low-magnesium treatment mimicking seizure-like activity/hyperexcitability in neurons (**a**; lower panel). Each trace represents $[Ca^{2+}]_c$ changes in a single neuron as measured with fura-2. Fibroblasts in culture co-stained with fluo-4 and TMRM (**b**). $Ca^{2+}$ oscillations are induced in fibroblasts loaded with caged $Ca^{2+}$ via intermittent UV exposure, triggering $Ca^{2+}$ released. This $Ca^{2+}$ release can be monitored by fluo-4. The trance in **c** represents $Ca^{2+}$ changes in a single fibroblast intermittently exposed to UV light. Arrows indicate time points when fibroblasts were exposed to UV light. Traces in **e** represent repetitive $Ca^{2+}$ oscillations (green trace, fluo-4) and $\Delta\Psi_m$ changes (red trace, TMRM) in a single fibroblast triggered by UV (**e**). Note that UV-induced $Ca^{2+}$ oscillations in fibroblasts (**e**) resemble those seen in neurons during seizure-like activity (**a**; lower panel). Repetitive $Ca^{2+}$ oscillations trigger $\Delta\Psi_m$ depolarisation in fibroblasts (**e**), whereas fibroblasts not stimulated with UV light do not show $\Delta\Psi_m$ depolarisation (**d**)

We developed an experimental approach to study mitochondrial function during dynamic $Ca^{2+}$ changes such as the ones observed during seizures and epilepsy. We here show that fibroblasts harbouring mutations in the mitochondrial genome have impaired ability to handle $Ca^{2+}$ in these models. This may explain why, particularly during periods of hyperexcitability, intracellular $Ca^{2+}$ levels cannot be compensated, leading to $Ca^{2+}$ overload and subsequent cell death in these diseases.

## Mitochondrial Membrane Potential in Cells Harbouring Mitochondrial DNA Mutations

We found decreased mitochondrial membrane potentials in fibroblasts harbouring mitochondrial DNA mutations. Previous studies have confirmed this, showing decreases in $\Delta\Psi$m in MT-TL1 and MT-TK mutations [22] and in ND6 point mutations [23]. Under pathological conditions as seen in anoxia, complex V works in a reverse mode, thus maintaining $\Delta\Psi$m at the expense of ATP consumption [22, 24]. Under these circumstances, blocking complex V with oligomycin depolarises the $\Delta\Psi$m. We have shown that this also applies to the mitochondrial mutations studied here. Whereas such reverse function of complex V has been observed in mitochondrial DNA (mtDNA) cybrid mitochondria harbouring mutation in the ND5 gene [23], we expand this to include fibroblasts with the same mutation in the ND5 gene and 8344A>G mutation in tRNA. Both a lower $\Delta\Psi$m and reverse mode functioning of complex V with ATP consumption in cells with mtDNA mutations are factors that should render these cells more vulnerable to $Ca^{2+}$-induced cell death and mitochondrial permeability transition pore opening. To confirm deficient oxidative phosphorylation in fibroblasts harbouring mtDNA mutations, we looked at NADH/$NAD^+$ ratios (redox indices) reflecting the activity of the mitochondrial electron transport chain. We found increased redox indices in cells harbouring mitochondrial mutations reflecting a deficiency of NADH to enter the electron transport chain.

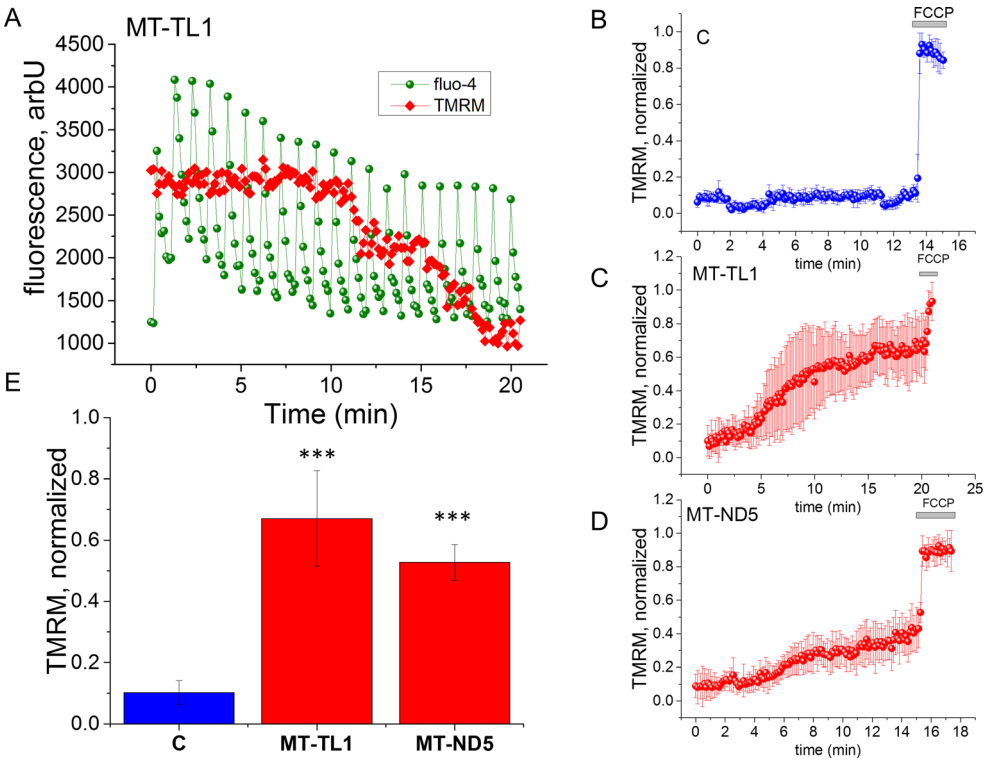


**Fig. 6** Impact of seizure-like oscillatory $Ca^{2+}$ changes on mitochondrial membrane potential in cells harbouring mitochondrial mutations. Decrease in TMRM fluorescence measured over the mitochondria after repetitive $Ca^{2+}$ challenge (**a**). TMRM fluorescence measured over cell nuclei shows a slight increase in control cells (**b**) whereas a significant increase was noted in cells harbouring mitochondrial mutations (**c**, **d**), indicating redistribution of the dye from depolarised mitochondria. Histogram quantifying an increase of TMRM fluorescence over nuclei in control cells and cells harbouring mitochondrial mutations (**e**); $***p < 0.001$

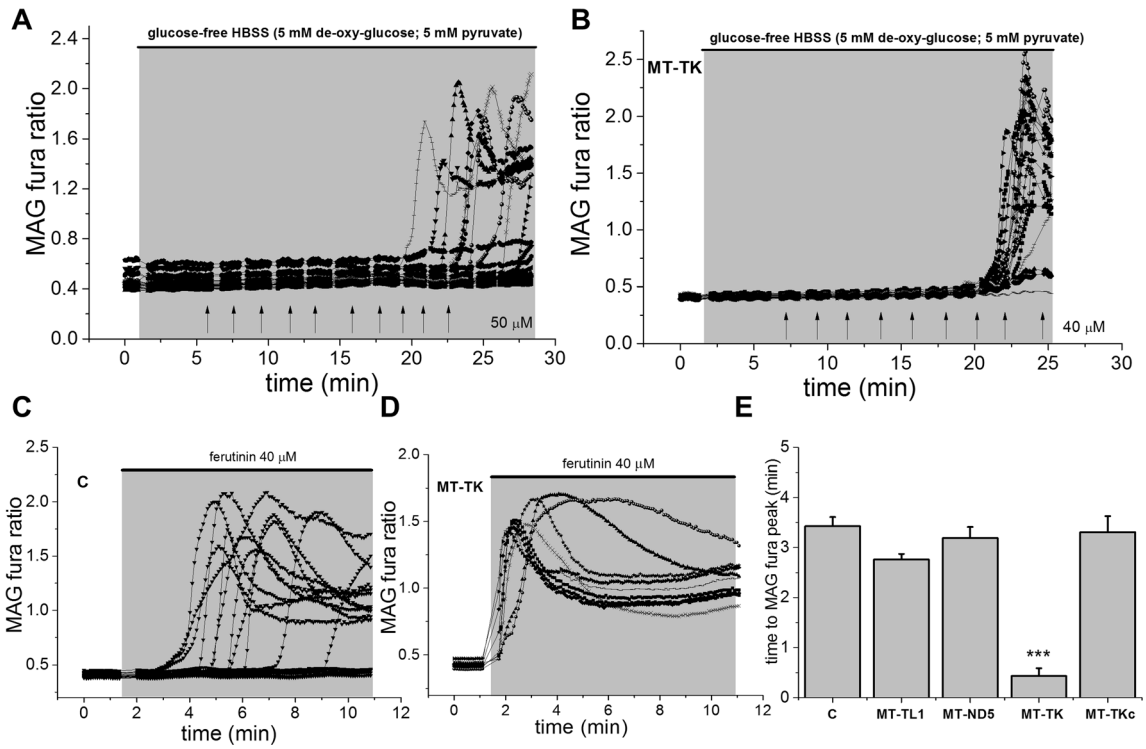


**Fig. 7** ATP depletion in fibroblasts with mitochondrial mutations. Increasing concentrations of ferutinin in glucose-free media lead to ATP depletion in fibroblast reflected by $[Mg^{2+}]_c$ increase. Traces in **a**–**d** represent a Mag-fura signal measured in a fibroblast. Each trace represents a fibroblast. Note that in control fibroblasts (**a**), lower ferutinin concentrations are required to induce ATP depletion when compared to fibroblasts harbouring the MT-TK mutation. Note that at the end of the 30-min interval, some captured control fibroblasts have not shown significant ATP depletion (**a**) whereas almost all fibroblasts with MT-TK mutation showed significant ATP depletion. Applying a single dose of ferutinin (40 μM) leads to ATP depletion in control fibroblasts (**c**) after a delay and immediate ATP depletion in fibroblasts harbouring the MT-TK mutation (**d**). Bar chart summarising (±SEM) delay in ATP depletion as measured by Mag-fura in different fibroblast cell lines (**e**); $***p < 0.001$

Despite this, NADH pools were low and NADH did not accumulate. This is likely to reflect an increase in glycolysis with transformation of pyruvate to lactate-consuming NADH. Increased glycolysis has been observed previously in cybrids from the patient suffering from mitochondrial disease due to ND5 gene mutation [23] and has been used as a—albeit unspecific—marker in the evaluation of mitochondrial disease in patients [25]. This glycolytic shift is also supported by previous data showing a decrease in mitochondrial respiration accompanied by increased glycolysis in fibroblasts with mitochondrial mutations as measured with the Seahorse Biosciences XFp extracellular flux analyser (Agilent Technologies, Santa Clara, USA) [26]. Decreased energetic substrates might fuel mitochondrial biogenesis, and we therefore asked whether the mitochondrial pool differed between the cell lines. There was no difference between the mitochondrial mass between the different fibroblasts. In keeping with our observations, James and colleagues found similar proportions of cell protein that sedimented in the mitochondrial fraction in fibroblast harbouring mitochondrial mutations (MELAS and MERRF) and control fibroblasts [22]. In addition, our results of ~ 10–15% of total cell mass occupied by mitochondria parallel their and previous findings [22, 27].

## $[Ca^{2+}]_c$ Stores in Cells Harbouring Mitochondrial DNA Mutations

We found differences in ER and mitochondrial $Ca^{2+}$ pools between the mutations (Fig. 3) which could be explained by the fact that $Ca^{2+}$ handling is not only determined by defects of oxidative phosphorylation, but it also depends on the site of the dysfunction and the severity of the defect. Mitochondrial $Ca^{2+}$ pools are affected differentially by the mutations which may be due to the severity of the respiratory chain compromise which is also reflected in the different NADH indices. ER pools are affected vice versa, pointing to a close link between ER $Ca^{2+}$ pools and mitochondrial $Ca^{2+}$ pools which is well known as both are organelles intimately linked to $Ca^{2+}$ homeostasis within the cell [13]. Interestingly, the MT-ND5 mutation which is characterised by a severe impairment in complex I showed decreased mitochondrial $Ca^{2+}$ stores whereas the tRNA mutations (MT-TL1 and MT-TK) showed increased mitochondrial $Ca^{2+}$ stores. There are links from the literature demonstrating that different mutations affect the complexes differentially. That is the MT-TL1 mutation results in respiratory defect arising from complex I and complex IV [28] whereas MT-TK mutation studied here has been shown to lead to a marked defect in overall mitochondrial translation [28, 29]. This may explain different phenotypical manifestations and also different effects on $Ca^{2+}$ handling which were found in our study.

## $[Ca^{2+}]_c$ Challenge Has Different Effects on the Mitochondrial Membrane Potential, PTP Opening and ATP Depletion-Induced Cell Collapse in Cells Harbouring Mitochondrial DNA Mutations and Controls

$Ca^{2+}$ signalling defects have been previously found to be perturbed in cybrids and neurons with mutations in the mitochondrial genome, and this effect was dependent on the mutation studied and was seen in mutations of mitochondrial tRNA and complex I and IV mutations [11, 30]. In normal cell metabolism, NADH dehydrogenase (complex I) can be stimulated by small concentrations of $Ca^{2+}$, leading to an increase in NADH turnover and, thus, hyperpolarisation of the $\Delta\Psi m$ [15, 31]. We found that a stepwise increase in the intracellular $Ca^{2+}$ concentration through ferutinin leads to a depolarisation of the $\Delta\Psi m$, whereas an increase or a steady $\Delta\Psi m$ was observed in controls (Fig. 4). $Ca^{2+}$-induced stepwise depolarisation of the $\Delta\Psi m$ was most evident in MT-ND5 fibroblast cell line, a mutation in the NADH dehydrogenase itself. Previous studies in the same cell line have suggested that this defect does not affect NADPH oxidase function itself but rather results in deficiency in proton pumping across the inner mitochondrial membrane [23]. This decrease in $\Delta\Psi_m$ was present—albeit to a lesser degree—in fibroblast MT-TL1 and MT-TK mutations, supporting previous reports [22]. A more compromised $\Delta\Psi_m$ implies more severe pathology which is in keeping with the clinical observation that mutations in the NADH dehydrogenase present with a more severe phenotype including epilepsy in their presentation [23, 32]. In addition, we were able to replicate this using $Ca^{2+}$ flash photolysis.

Further, previous reports show that the A3243G mutation disrupts 5-taurinomethyluridine (lacked τm5U modification) in mitochondrial tRNA, leading to UUG codon-specific decoding difficulties. UUG codon usage in the 13 proteins encoded by mtDNA is low, with one exception; namely, ND6 gene encoding complex I contains eight UUG codons which form 42% of total ND6 codons in ND6 [33, 34]. This explains why complex I translation is markedly reduced in this mutation whereas other mitochondrial complexes or proteins are relatively preserved [28, 33]. Our data show that the $\Delta\Psi m$ after $Ca^{2+}$ challenge of fibroblasts with the A3243G mutation remained relatively stable, and the time point of PTP opening was comparable to control cell lines. This may be explained by a partially functional complex I and also by possible compensation by other complexes which maintain the $\Delta\Psi m$.

Mutations in tRNALys such as A8344G, on the other hand, severely disrupt protein synthesis of several proteins involved in oxidative phosphorylation [28, 29, 35]. This graded insufficient mitochondrial protein expression with ND6 mutations at the severe end of the spectrum, followed by 8344A>G mutation (MT-TK fibroblasts) and by 3243A>G mutations

(MT-TL1 fibroblasts) presenting partial complex I deficiency, is mirrored in our findings of graded ΔΨm decrease with increasing $Ca^{2+}$ challenge. Differences in MPTP opening indicated by a rapid loss of ΔΨm were only observed in the MT-ND5 fibroblast cell line which showed a rapid ΔΨm decline after repeated $Ca^{2+}$ challenges, indicating that a critical depolarisation needs to be reached prior to MPTP opening (Fig. 5b). It should be noted that differences in $Ca^{2+}$ handling were picked up with $Ca^{2+}$ flash photolysis in the MT-TL1 mutation which may point to different sensitivities of these models which, as such, may be used as complementary.

Interestingly, the MT-TK cell line (A8344G) was characterised by high ATP consumption. This can be explained by FiF0ATPase working in reverse mode which is confirmed by the fact that oligomycin leads to a marked depolarisation of the mitochondrial membrane potential in these cells (Fig. 1c, d). In addition, this cell line shows very low NADH pools (Fig. 2b) and high mitochondrial $Ca^{2+}$ (Fig. 3c). Taken together, all these changes predispose to ATP depletion and cell collapse in the experiments performed (Fig. 7).

### Relation of the Changes Modelled Here to $Ca^{2+}$ Homeostasis and Neuronal Cell Death During Seizures

There is strong evidence that $Ca^{2+}$ homeostasis is conserved among vertebral mitochondria and among mitochondria of different tissues within a single species [12]. This is likely due to the fact that respiration which is strongly linked to mitochondria plays a general and fundamental role in all vertebrate tissues. We here found a $Ca^{2+}$-dependent depolarisation of the mitochondrial membrane potential, leading to MPTP opening and cell collapse in fibroblasts challenged with repetitive $Ca^{2+}$ overload. It is well known that lowering of the mitochondrial potential and ATP depletion can lead to lowering of the threshold of PTP opening and thereby increase the risk of $Ca^{2+}$-induced cell death [36]. The changes modelled here, therefore, may serve as an explanation for enhanced neuronal cell death in patients suffering from epilepsies due to mitochondrial mutations [37]. Excessive $Ca^{2+}$ oscillations, which are the cellular signature of epileptiform activity, impose a metabolic burden on the cell [7]. This is due to mitochondrial $Ca^{2+}$ buffering which competes with ATP generation and due to the need to restore cellular $Ca^{2+}$ homeostasis, a process which is dependent on energetic molecules such as ATP. We here show that such oscillations induce mitochondrial membrane potential changes, which ultimately may lead to cell death, more readily in cells which are affected by mitochondrial mutations. This provides an insight into mechanisms of cell death in these conditions. In addition, more recently, mutations in the mitochondrial genome have been identified in tissue samples from patients suffering from common types of epilepsy such as hippocampal sclerosis [38] which may indicate that these mechanisms also apply to more common epilepsy syndromes.

## Limitations, Conclusions and Future Outlook

We acknowledge that fibroblasts are limited to that extent that they cannot reproduce several aspects of seizure activity such as occurs in the human brain in vivo, and that they are conceptually different from neurons. In a way, all epilepsy models just model some aspects of seizure activity and epilepsy but are deficient in modelling the full spectrum of human disease [39]. Metabolic changes, changes in $Ca^{2+}$ handling and changes in ROS occur during seizures [40, 41], and the approach chosen here is meant to model one aspect of the disease, namely impaired $Ca^{2+}$ handling such as we have found before in neurons during seizure-like activity [7]. More recently, disease assays have been developed which demonstrate that metabolic changes in mutations leading to epileptic phenotypes can be reliably detected in e.g. zebrafish model of Dravet syndrome [42] and that such platforms can also serve for drug screening and unravel new drug targets [42, 43]. Such screening models are needed to allow high-throughput screening and personalised screening for the treatment of epilepsy. The model proposed here is one step forward toward such models and identifies deficient $Ca^{2+}$ homeostasis as a potential readout.

## Material and Methods

### Fibroblast Lines

A total of five fibroblast cell lines were used for this study. Three fibroblast lines were generated from biopsies taken following patients' informed consent and ethical approval from the National Hospital for Neurology and Neurosurgery/Institute of Neurology Joint Research Ethics Committee (London, UK). The other two fibroblast lines were kindly provided by the MRC Centre for Neuromuscular Diseases BioBank London. The study lines included control fibroblasts, fibroblasts with the 3243A>G mutation in encoded mitochondrial tRNA leucine 1 (UUA/G) (MT-TL1), 13528A>G and 13565C>T mutations in encoded mitochondrial NADH dehydrogenase 5 (MT-ND5), 8344A>G mutation in encoded mitochondrial tRNA lysine (MT-TK) and, finally, fibroblasts from the unaffected mother of the MT-TK patient that serve as control (MT-TKc). Patients' clinical details are available in Suppl. Table 1. The rationale for choosing these mutations was that these mutations are a leading cause for mitochondrial disease and are the main mutations found in MELAS and MERRF. Half of the pathogenic mutations in mtDNA map to mtRNA genes [44]. The mutation 3243A>G accounts for 80% of patients suffering from MELAS [3, 45]

and results in a translational depression of the ND6 (a subcomplex of complex I of the respiratory chain) and thus explains a decrease in complex I activity seen in these patients [34]. In addition, the mutations 13528A>G and 13565C>T, whereas rare, are known to affect the ND5 subunit of complex I (MT-ND5). Fibroblasts of this patient have been studied before [23]. Mutation load in the mother's fibroblasts is 44% compared to mutation load in the patient which is 82%. Quantification of the proportion of the mutant mtDNA for each fibroblast cell line is presented in Suppl. Table 1. We want to highlight that the methods used in this paper rely on analyses of single cell and single mitochondrion. Thus, it is expected that these methods are more sensitive than conventional enzyme assays which are usually done in cell suspensions. Thus, even low levels of mutation load are likely to translate into biological effects seen via live cell imaging. In addition, a previous study which investigated the effects of MT-TL1 mutation on mitochondrial membrane potential has confirmed this, showing that a low mutation load (of < 50%) had an impact on the mitochondrial membrane potential [22].

## Fibroblast Cultures

Fibroblast lines were generated from ~ 4-mm punch biopsies taken under local anaesthesia (1–2 ml of 1% lidocaine) following informed consent. Biopsies were dissected and cultivated in 5-cm petri dishes in Dulbecco's modified Eagle's medium (DMEM; GlutaMAX, Invitrogen) supplemented with 10% FBS and 1% (*v*/*v*) penicillin/streptomycin at 37 °C in 5% humidified $CO_2$ to allow fibroblast outgrowth. Once fibroblasts reached confluency, cells were detached with TrypLE (Invitrogen) and transferred to T75 tissue culture flasks for further expansion and cryopreservation. For all experiments, fibroblasts were plated onto 22-mm coverslips 24 h prior to experiments. All cells were kept at a comparable passage number (± 2 passages), and experiments were always run in parallel with control. All experiments were normalised to C.

## Measurement of Mitochondrial Membrane Potential ($\Delta\Psi_m$)

Fibroblasts were loaded with 25 nM TMRM in a HEPES-buffered salt solution (HBSS, Invitrogen). Cells were incubated for 50 min prior to experiments to allow for equilibration of TMRM which is achieved late into the incubation process. This concentration of TMRM allows imaging of TMRM in *redistribution mode*, and thus, a reduction in mitochondrion-localised TMRM fluorescence represents mitochondrial depolarisation. At the same time, reduction of the TMRM fluorescent signal leads to a mild increase in TMRM cytosolic signal due to redistribution of the dye. This redistribution also occurs across the plasma membrane, and thus, an initial rise of cytosolic TMRM is followed by a slow steady decline due to redistribution across the plasma membrane (Suppl. Fig. 2). This redistribution kinetic allows visualising the velocity of TMRM redistribution by plotting the cytosolic TMRM fluorescence changes. A peak of the TMRM signal thus indicates fastest TMRM redistribution and, therefore, was taken as an indicator of permeability transition pore opening in our experiments (Suppl. Fig. 2). The dye was kept in the solution throughout the experiment. Confocal images were acquired using a Zeiss 710 VIS CLSM (Zeiss, Oberkochen, Germany) equipped with a META detection system and a × 40 oil immersion objective. Excitation of the dye was through the 560-nm laser, and fluorescence was measured above 580 nm. For all experiments, the confocal microscope illumination intensity was kept to a minimum (at 0.2% of laser output) to avoid phototoxicity and the pinhole was set to give an optical slice of ~ 2 μm. TMRM fluorescence was measured over the mitochondria only and is therefore independent of the mitochondrial mass or density. We automated choice of regions of interest within the mitochondria and automated removal of the background using Volocity 3D image analysis software (PerkinElmer).

Basal $\Delta\Psi_m$ as shown in Fig. 1 was measured by recording Z-stack images whereas the kinetic response of $\Delta\Psi_m$ to mitochondrial toxins as shown in Fig. 1b–e was obtained as a time series recording in a single plane.

## Measurement of NADH Redox Indices

An epifluorescence inverted microscope equipped with a × 20 fluorite objective was used to measure NADH autofluorescence. The microscope is fitted with a xenon arc lamp and a monochromator (Cairn Research, Faversham, Kent, UK). Excitation light for the experiments was 350 nm, and emission fluorescence was captured through a 455-nm long-pass filter to a cooled CCD camera (Retiga, QImaging, Surrey, BC, Canada) and digitised to 12-bit resolution.

## Measurement of Mitochondrial Mass

To determine the mitochondrial mass, cells were loaded with 25 nM TMRM and CellTrace Calcein Blue AM (5 μM; Invitrogen) and 0.005% pluronic for 40 min. Z-stack confocal images were acquired using a Zeiss 710 VIS CLSM (Zeiss, Oberkochen, Germany), equipped with a META detection system and a × 40 oil immersion objective. Excitation of the dye was through the 560-nm laser for TMRM and the 405-nm laser for calcein blue, and fluorescence emission was measured above 580 nm. Mitochondrial mass was computed as the ratio of the volume of the mitochondrial network (determined by TMRM fluorescence) divided by the volume of the fibroblast (determined as calcein blue fluorescence) expressed in percentages. Images were autocontrasted separately to allow definition of the mitochondrial network independent of

the ΔΨm. Volumes were determined using Volocity 3D image analysis software (PerkinElmer).

## Measurement of $[Ca^{2+}]_c$ Pools

For measurements of mitochondrial and ER $Ca^{2+}$ pools, cells were loaded with fura-2 AM and 0.005% pluronic in a HEPES-buffered solution. Fibroblasts were incubated for 30 min prior to experiments, and experiments were performed in a $Ca^{2+}$-free HEPES-buffered solution. $[Ca^{2+}]_c$ was measured in a single fibroblast using excitation light provided by a xenon arc lamp, the beam passing through a monochromator at 340 and 380 with bandwidth of 10 nm (Cairn Research, Kent, UK). Emitted fluorescent light passed through a 515-nm long-pass filter to a cooled CCD camera (Retiga; QImaging) and was digitised to 12-bit resolution. $Ca^{2+}$ imaging data was acquired at a frame interval of 10 s and analysed using software from Andor (Belfast, UK). Traces were computed and plotted as fura-2 ratio of excitation acquired at 340 and 380 nm, both with emission at > 515 nm. Fura ratio was not calibrated due to inaccuracies arising from different calibration methods.

Co-measurements of $\Delta\Psi_m$ and $[Ca^{2+}]_c$ were performed using TMRM and fluo-4. The TMRM staining method is explained above. Fibroblasts were incubated with TMRM and fluo-4 and 0.005% pluronic in a HEPES-buffered solution for 40 min. Incubation solution was replaced with fresh HEPES-buffered solution and 25 nM TMRM prior to experiments. TMRM and fluo-4 fluorescence was measured on a confocal microscope using a × 64 objective to allow visualisation of a single mitochondrion. In addition to the laser settings required to capture TMRM fluorescence (see above), fluo-4 was excited with the 488 laser and emission light was measured at 505–550 nm.

## Measurement of ATP Levels and Cell Collapse as Indicated by Massive $[Ca^{2+}]_c$ Increases

Kinetic ATP changes and massive $[Ca^{2+}]_c$ in fibroblasts were determined indirectly by measuring free intracellular $[Mg^{2+}]_c$ and free intracellular $[Ca^{2+}]_c$ simultaneously. $Mg^{2+}$ is released from $Mg^{2+}$-ATP due to consumption of ATP, and therefore, $Mg^{2+}$ increase can be seen as a surrogate marker of intracellular ATP decrease. To measure $[Mg^{2+}]_c$, we used the ratiometric dye Mag-fura (Invitrogen). Mag-fura is a high-affinity $Mg^{2+}$ indicator and a low-affinity $Ca^{2+}$ indicator. This is critical since in situations with massive ATP depletion, ionic homeostasis will be affected, resulting in a $Ca^{2+}$ overload of the cell. This will result in a massive increase in Mag-fura fluorescence, signifying an energetic collapse of the cell. We made use of this dual function of Mag-fura, i.e. measurement of basal ATP levels and energetic collapse (see Fig. 7). Fibroblasts were incubated with Mag-fura AM and 0.001% pluronic for 30 min prior to experiments. Fluorescent images were obtained with the same settings as outlined for fura-2 AM measurements and expressed as ratios (340:380 Mag-fura ratio). The delay to energetic collapse was determined for each fibroblast by determining the *x*-coordinate (time) of the maximum slope of the Mag-fura signal (see Fig. 7).

## $Ca^{2+}$ Flash Photolysis

For imaging of $\Delta\Psi_m$ and $Ca^{2+}$ during flash photolysis, a Zeiss 510 UV–vis CLSM equipped with a META detection system and a × 40 oil immersion objective was used. Caged $Ca^{2+}$, 10 μM *o*-nitrophenyl EGTA and AM (NP-EGTA, AM) were incubated at the same time as fluo-4 and TMRM, and $Ca^{2+}$-free medium containing 0.5 mM EGTA [46]. Flashes were delivered to a region of interest, which was defined prior to the experiments, targeting a single cell. Flashes were delivered at a rate of 1 flash per min. $Ca^{2+}$ increase was verified by recording qualitative $Ca^{2+}$ changes with fluo-4. Excitation and emission spectra were similar as those outlined above for TMRM and fluo-4.

## Statistical Analyses

Statistical analyses (one-way ANOVA, Dunnett's test) were performed using SPSS 17.0 (Chicago, IL, USA). The significance level was set at $p < 0.05$, and all data are given as mean ± standard error of the mean (SEM). Post hoc calculations were computed to compare the difference to C.

**Acknowledgements** The authors would like to thank the MRC Centre for Neuromuscular Diseases BioBank London for providing the additional fibroblast lines for this study.

**Author Contributions** SK and AYA conceived the study. SK performed and designed the experiments. EP and HH contributed toward the experiments. SK and AYA analysed the data. SK, AYA and MCW wrote the manuscript. All authors critically discussed the data and approved the final version of the manuscript.

**Funding Information** This work was supported by the Medical Faculty of the University of Münster (17-003 fellowship to SK) and the NIHR Queen Square Dementia Biomedical Research Unit. This work was undertaken at UCLH/UCL which receives a proportion of funding from the Department of Health's NIHR Biomedical Research Centres funding scheme.

## References

1. Schapira AHV (2012) Mitochondrial diseases. Lancet 379:1825–1834
2. Abbott JA, Francklyn CS, Robey-Bond SM (2014) Transfer RNA and human disease. Front Genet 5:158
3. Goto Y, Nonaka I, Horai S (1990) A mutation in the tRNA(Leu)(UUR) gene associated with the MELAS subgroup of mitochondrial encephalomyopathies. Nature 348:651–653

4. Shoffner JM, Lott MT, Lezza AM, Seibel P, Ballinger SW, Wallace DC (1990) Myoclonic epilepsy and ragged-red fiber disease (MERRF) is associated with a mitochondrial DNA tRNA(Lys) mutation. Cell 61:931–937
5. Schapira AHV (2006) Mitochondrial disease. Lancet 368:70–82
6. Canafoglia L, Franceschetti S, Antozzi C, Carrara F, Farina L, Granata T, Lamantea E, Savoiardo M et al (2001) Epileptic phenotypes associated with mitochondrial disorders. Neurology 56: 1340–1346
7. Kovac S, Domijan A-M, Walker MC, Abramov AY (2012) Prolonged seizure activity impairs mitochondrial bioenergetics and induces cell death. J Cell Sci 125:1796–1806
8. Kovac S, Domijan A-M, Walker MC, Abramov AY (2014) Seizure activity results in calcium- and mitochondria-independent ROS production via NADPH and xanthine oxidase activation. Cell Death Dis 5:e1442
9. Williams S, Hamil N, Abramov AY, Walker MC, Kovac S (2015) Status epilepticus results in persistent overproduction of reactive oxygen species, inhibition of which is neuroprotective. Neuroscience 303:160–165
10. Moudy AM, Handran SD, Goldberg MP, Ruffin N, Karl I, Kranz-Eble P, DeVivo DC, Rothman SM (1995) Abnormal calcium homeostasis and mitochondrial polarization in a human encephalomyopathy. Proc Natl Acad Sci U S A 92:729–733
11. Trevelyan AJ, Kirby DM, Smulders-Srinivasan TK, Nooteboom M, Acin-Perez R, Enriquez JA, Whittington MA, Lightowlers RN et al (2010) Mitochondrial DNA mutations affect calcium handling in differentiated neurons. Brain 133:787–796
12. Carafoli E, Lehninger AL (1971) A survey of the interaction of calcium ions with mitochondria from different tissues and species. Biochem J 122:681–690
13. Szabadkai G, Duchen MR (2008) Mitochondria: the hub of cellular $Ca^{2+}$ signaling. Physiology (Bethesda) 23:84–94
14. Denton RM, McCormack JG, Edgell NJ (1980) Role of calcium ions in the regulation of intramitochondrial metabolism. Effects of $Na^{+}$, $Mg^{2+}$ and ruthenium red on the $Ca^{2+}$-stimulated oxidation of oxoglutarate and on pyruvate dehydrogenase activity in intact rat heart mitochondria. Biochem J 190:107–117
15. Nicholls DG (2005) Mitochondria and calcium signaling. Cell Calcium 38:311–317
16. Rizzuto R, Pinton P, Carrington W, Fay FS, Fogarty KE, Lifshitz LM, Tuft RA, Pozzan T (1998) Close contacts with the endoplasmic reticulum as determinants of mitochondrial $Ca^{2+}$ responses. Science 280:1763–1766
17. DeLorenzo RJ, Sun DA (2006) Basic mechanisms in status epilepticus: role of calcium in neuronal injury and the induction of epileptogenesis. Adv Neurol 97:187–197
18. Abramov AY, Zamaraeva MV, Hagelgans AI, Azimov RR, Krasilnikov OV (2001) Influence of plant terpenoids on the permeability of mitochondria and lipid bilayers. Biochim Biophys Acta 1512:98–110
19. Zamaraeva MV, Hagelgans AI, Abramov AY, Ternovsky VI, Merzlyak PG, Tashmukhamedov BA, Saidkhodzjaev AI (1997) Ionophoretic properties of ferutinin. Cell Calcium 22:235–241
20. Abramov AY, Duchen MR (2003) Actions of ionomycin, 4-BrA23187 and a novel electrogenic $Ca^{2+}$ ionophore on mitochondria in intact cells. Cell Calcium 33:101–112
21. Abramov AY, Duchen MR (2010) Impaired mitochondrial bioenergetics determines glutamate-induced delayed calcium deregulation in neurons. Biochim Biophys Acta 1800:297–304
22. James AM, Wei YH, Pang CY, Murphy MP (1996) Altered mitochondrial function in fibroblasts containing MELAS or MERRF mitochondrial DNA mutations. Biochem J 318:401–407
23. McKenzie M, Liolitsa D, Akinshina N, Campanella M, Sisodiya S, Hargreaves I, Nirmalananthan N, Sweeney MG et al (2007) Mitochondrial ND5 gene variation associated with encephalomyopathy and mitochondrial ATP consumption. J Biol Chem 282:36845–36852
24. Appleby RD, Porteous WK, Hughes G, James AM, Shannon D, Wei YH, Murphy MP (1999) Quantitation and origin of the mitochondrial membrane potential in human cells lacking mitochondrial DNA. Eur J Biochem 262:108–116
25. Mitochondrial Medicine Society's Committee on Diagnosis, Haas RH, Parikh S, Falk MJ, Saneto RP, Wolf NI, Darin N, Wong L-J et al (2008) The in-depth evaluation of suspected mitochondrial disease. Mol Genet Metab 94:16–37
26. Invernizzi F, D'Amato I, Jensen PB, Ravaglia S, Zeviani M, Tiranti V (2012) Microscale oxygraphy reveals OXPHOS impairment in MRC mutant cells. Mitochondrion 12:328–335
27. Rugolo M, Lenaz G (1987) Monitoring of the mitochondrial and plasma membrane potentials in human fibroblasts by tetraphenylphosphonium ion distribution. J Bioenerg Biomembr 19:705–718
28. Suzuki T, Nagao A, Suzuki T (2011) Human mitochondrial tRNAs: biogenesis, function, structural aspects, and diseases. Annu Rev Genet 45:299–329
29. Enriquez JA, Chomyn A, Attardi G (1995) MtDNA mutation in MERRF syndrome causes defective aminoacylation of tRNA(Lys) and premature translation termination. Nat Genet 10:47–55
30. Brini M, Pinton P, King MP, Davidson M, Schon EA, Rizzuto R (1999) A calcium signaling defect in the pathogenesis of a mitochondrial DNA inherited oxidative phosphorylation deficiency. Nat Med 5:951–954
31. McCormack JG, Halestrap AP, Denton RM (1990) Role of calcium ions in regulation of mammalian intramitochondrial metabolism. Physiol Rev 70:391–425
32. Ravn K, Wibrand F, Hansen FJ, Horn N, Rosenberg T, Schwartz M (2001) An mtDNA mutation, 14453G→A, in the NADH dehydrogenase subunit 6 associated with severe MELAS syndrome. Eur J Hum Genet 9:805–809
33. Dunbar DR, Moonie PA, Zeviani M, Holt IJ (1996) Complex I deficiency is associated with 3243G:C mitochondrial DNA in osteosarcoma cell cybrids. Hum Mol Genet 5:123–129
34. Kirino Y, Yasukawa T, Ohta S, Akira S, Ishihara K, Watanabe K, Suzuki T (2004) Codon-specific translational defect caused by a wobble modification deficiency in mutant tRNA from a human mitochondrial disease. Proc Natl Acad Sci U S A 101:15070–15075
35. Yasukawa T, Suzuki T, Ishii N, Ohta S, Watanabe K (2001) Wobble modification defect in tRNA disturbs codon-anticodon interaction in a mitochondrial disease. EMBO J 20:4794–4802
36. Bernardi P, Petronilli V, Di Lisa F, Forte M (2001) A mitochondrial perspective on cell death. Trends Biochem Sci 26:112–117
37. Sparaco M, Bonilla E, DiMauro S, Powers JM (1993) Neuropathology of mitochondrial encephalomyopathies due to mitochondrial DNA defects. J Neuropathol Exp Neurol 52:1–10
38. Gurses C, Azakli H, Alptekin A, Cakiris A, Abaci N, Arikan M, Kursun O, Gokyigit A et al (2014) Mitochondrial DNA profiling via genomic analysis in mesial temporal lobe epilepsy patients with hippocampal sclerosis. Gene 538:323–327
39. Walker MC, Kovac S (2015) Seize the moment that is thine: how should we define seizures? Brain 138:1127–1128
40. Kovac S, Dinkova Kostova AT, Herrmann AM, Melzer N, Meuth SG, Gorji A (2017) Metabolic and homeostatic changes in seizures and acquired epilepsy-mitochondria, calcium dynamics and reactive oxygen species. Int J Mol Sci 18
41. Kovac S, Dinkova-Kostova AT, Abramov AY (2016) The role of reactive oxygen species in epilepsy. Reactive Oxygen Species 1: 38–52
42. Kumar MG, Rowley S, Fulton R, Dinday MT, Baraban SC, Patel M (2016) Altered glycolysis and mitochondrial respiration in a zebrafish model of Dravet syndrome. eNeuro 3

43. Ibhazehiebo K, Gavrilovici C, de la Hoz CL, Ma S-C, Rehak R, Kaushik G, Meza Santoscoy PL, Scott L et al (2018) A novel metabolism-based phenotypic drug discovery platform in zebrafish uncovers HDACs 1 and 3 as a potential combined anti-seizure drug target. Brain 141:744–761. https://doi.org/10.1093/brain/awx364
44. Brandon MC, Lott MT, Nguyen KC, Spolim S, Navathe SB, Baldi P, Wallace DC (2005) MITOMAP: a human mitochondrial genome database—2004 update. Nucleic Acids Res 33:D611–D613
45. Kobayashi Y, Momoi MY, Tominaga K, Momoi T, Nihei K, Yanagisawa M, Kagawa Y, Ohta S (1990) A point mutation in the mitochondrial tRNA(Leu)(UUR) gene in MELAS (mitochondrial myopathy, encephalopathy, lactic acidosis and stroke-like episodes). Biochem Biophys Res Commun 173:816–822
46. Gandhi S, Wood-Kaczmar A, Yao Z, Plun-Favreau H, Deas E, Klupsch K, Downward J, Latchman DS et al (2009) PINK1-associated Parkinson's disease is caused by neuronal vulnerability to calcium-induced cell death. Mol Cell 33:627–638